European Journal of Pharmaceutics and Biopharmaceutics 145 (2019) 54–64

Contents lists available at ScienceDirect

European Journal of Pharmaceutics and Biopharmaceutics

journal homepage: www.elsevier.com/locate/ejpb

Sequentially dynamic polymeric micelles with detachable PEGylation for enhanced chemotherapeutic efficacy

Guoqing Yan[1], Yan Huang[1], Dapeng Li, Yong Xu, Jun Wang, Xin Wang, Rupei Tang*

Engineering Research Center for Biomedical Materials, School of Life Science, Anhui University, 111 Jiulong Road, Hefei, Anhui Province 230601, PR China

ARTICLE INFO

Keywords:
Micelles
Dual stimuli
Detachable PEGylation
Size transition
Antitumor

ABSTRACT

To achieve enhanced cancer therapy, a sequentially dynamic polymeric drug delivery system (ortho ester-linked PEGylated poly(disulfide)s-based micelle-doxorubicin (PS-*g*-OEMPEG-DOX)) is successfully constructed. The PEGylated micelle can keep stable in sodium dodecyl sulfate (SDS) solution at pH 7.4, but be prone to DePEGylation and dynamic size changes via the hydrolysis of ortho ester linkages in side chains at tumoral extracellular pH value (6.5). Moreover, the micelle can rapidly release DOX via the cleavage of poly(disulfide)s in backbone at intracellular reductive milieu (10 mmol/L of dithiothreitol (DTT)). The dynamic micelle with detachable PEGylation achieves the stable blood circulation, improved cellular uptake and cytotoxicity, stronger in vitro penetration and inhibition of tumoral multicellular spheroids, and significant in vivo tumor accumulation and inhibition while decreasing side effects. Thus, the sequentially dynamic polymeric micelle with detachable PEGylation can be considered as a promising and effective drug delivery system in cancer therapy.

1. Introduction

Polymeric drug delivery systems have been developed to improve the cancer therapy of conventional chemotherapeutic drugs [1]. Some of these polymeric systems such as nanoparticle albumin-bound paclitaxel, liposomal daunorubicin and PEGylated liposomal doxorubicin have been clinically used [2,3], and approve so far minimal toxicity and easier tumor accumulation via tumoral enhanced permeability and retention (EPR) effect [4,5]. However, they fail to significantly improve the overall survival of patients due to their single function [5,6]. Thus, there is an imperious demand to develop a multifunctional polymeric drug delivery system to achieve enhanced cancer therapy.

PEGylated polymeric delivery systems such as PEGylated liposomal doxorubicin is highly desirable, because they played a crucial role in stabilizing nanoparticles, protecting themselves from clearance by reticuloendothelial system (RES) and increasing blood circulation [7,8]. However, their cellular uptake might be hampered by PEGylation upon arrival at target tumor sites [9]. This dilemma could be suppressed via detachable PEG shielding strategy under different physiological environments [10–13]. For example, Wang and colleagues designed a tumor acidity-sensitive polymeric vector, whose PEG shell can keep stable at physiological pH (~7.4), but be removed via linkage breakage of 2-propionic-3-methylmaleic anhydride at tumoral extracellular pH (~6.5–7.0) [11,13]. Moreover, the particle size of a polymeric delivery system is an important nano-property to affect tumor accumulation, which can be improved by dynamic size change at tumor sites [14,15]. Thus, an ideal drug carrier with DePEGylation following size transitions at tumoral extracellular pH can enhance both tumor accumulation and cellular uptake. Our group has successfully designed a series of ultra-pH-sensitive poly(ortho ester)s-based drug delivery systems with dynamic size changes at tumoral extracellular pH [16–19]. Therefore, such dynamic polymeric delivery system with detachable PEG shielding strategy could be obtained by linking PEG with ortho ester bond. In addition, the tumoral intracellular drug release is still required to be programmed for enhanced cytotoxicity.

Reduction-sensitive polymeric drug delivery systems have been recently aroused wide concern, and most of them have successfully achieved tumoral intracellular programmable drug release [20,21]. Disulfide linkage as characteristic reduction-sensitive bond can be stable enough in the blood circulation and extracellular microenvironment, but easily cleaved in the intracellular reductive milieu via exchange reactions between thiol and disulfide [22,23]. In this work, a dual sensitive polymeric drug delivery system may be achieved by the tunable chemical bonding of poly(disulfide)s in backbones and ortho ester-linked PEG in side chains, thus realizing a sequentially dynamic drug delivery to tumor cells from blood vessels (Scheme 1).

* Corresponding author.
E-mail address: tangrp99@iccas.ac.cn (R. Tang).
[1] Guoqing Yan and Yan Huang contributed equally.

https://doi.org/10.1016/j.ejpb.2019.10.009
Received 11 July 2019; Received in revised form 9 October 2019; Accepted 21 October 2019
Available online 22 October 2019
0939-6411/

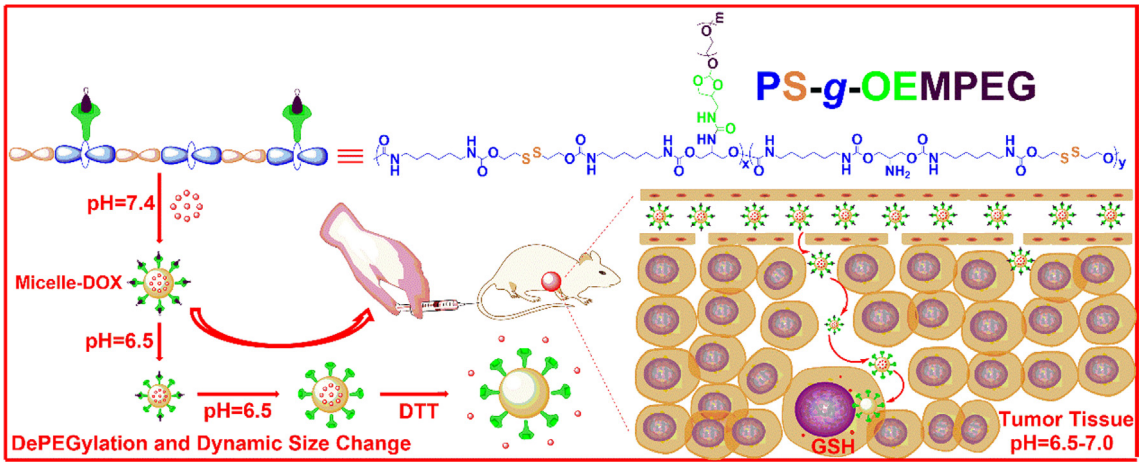

Scheme 1. The sequentially dynamic drug delivery to tumor cells of PS-*g*-OEMPEG-DOX.

2. Material and methods

2.1. Materials

Dichloromethane (DCM), dimethyl sulfoxide (DMSO), dimethyl formamide (DMF) and triethylamine (TEA) were dehydrated by CaH_2 before use. Pyridinium p-toluene sulfonate acid (Py-PTSA), 2-hydroxyethyl disulfide (2-HDS), N,N′-carbonyldiimidazole (CDI), dibutyltin dilaurate (DBTDL), methoxypolyethylene glycol (MPEG) (Mw = 2000), doxorubicin hydrochloride (DOX·HCl), hexamethylene diisocyanate (HDI) and dithiothreitol (DTT) were obtained from Sigma-Aldrich (China). 2,2,2-Trifluoro-N-(2-methoxy-1,3-dioxolan-4-ylmethyl) acetamide (TA) was synthesized and purified as previously described [24]. Human liver carcinoma cell line (HepG2) and murine hepatic cancer cell line (H22) were obtained from Shanghai Institute of Cell Biology (Shanghai, China). Male ICR mice (18–22 g) were purchased from Animal Center of Anhui Medical University (Hefei, China), and used in the Guide of Experimental Animal Ethics Committee of Anhui University.

2.2. Synthesis of (2-(2-O-MPEG)-1,3-dioxolan-4-yl)methanamine (MN)

A mixture of TA (2.29 g, 10.00 mmol), MPEG (29.99 g, 15.00 mmol) and Py-PTSA (0.027 g, 0.06 mmol) was refluxed in toluene (100 mL) under the protection of nitrogen at 115 °C for 8 h. After concentration via vacuum distillation, the product was dissolved in 100 mL of CDM, and extracted with saturated NaCl. The CDM layer was dehydrated over anhydrous $MgSO_4$, condensed and stirred in NaOH solution (20 mL, 1.00 mol/L) for 5 h in turn. Finally, the mixture was extracted with CDM twice, dehydrated over $MgSO_4$ and condensed to obtain a white powder (16.46 g, 78.3%). Its structure was determined via ^{1}H NMR in $CDCl_3$ using a Bruker AM-400 MHz spectrometer (Bruker Biospin).

2.3. Synthesis of MPEG 1H-imidazole-1-carboxylate (MIC)

In the nitrogen atmosphere, MPEG (20.00 g, 10.00 mmol) and CDI (2.43 g, 15.00 mmol) were dissolved in anhydrous DCM (100 mL), and vigorously stirred at 25 °C for 24 h. Afterwards, the crude product was extracted using saturated NaCl solution and the CDM layer was dehydrated over anhydrous $MgSO_4$. The product as a white powder (17.40 g, 83.1%) was yielded after concentration by a rotary evaporator, whose structure was confirmed via ^{1}H NMR in $CDCl_3$.

2.4. Synthesis of poly (disulfide)s with primary amines in side chains (PS-g-NH_2)

A mixture of N-(1,3-dihydroxypropan-2-yl)- 2,2,2-trifluoroacetamide (0.67 g, 3.58 mmol), 2-HDS (0.55 g, 3.58 mmol), HDI (1.20 g, 7.16 mmol) and a catalytic amount of DBTDL was vigorously stirred in 10 mL of anhydrous DMSO at 65 °C for 24 h under nitrogen atmosphere, and then precipitated in cold diethyl ether. The product (PS-*g*-F3) was dried by vacuum distillation. Afterwards, PS-*g*-F_3 was dissolved in 50 mL of tetrahydrofuran, and poured into 7% Na_2CO_3 solution. The mixture was vigorously stirred for 6 h and dialyzed (MWCO 3500) against distilled deionized for 24 h. Finally, PS-*g*-NH_2 was obtained by lyophilization as a white solid (1.36 g, 65.7%), whose structure was confirmed via ^{1}H NMR in DMSO-d_6.

2.5. Synthesis of PEGylated poly (disulfide)s (PS-g-OEMPEG and PS-g-MPEG)

In nitrogen atmosphere, NM-active ester (1.16 g, 0.52 mmol) synthesized via reaction between NM and CDI at the molar ratio of 1–1.5, was added to a stirred mixture of PS-*g*-NH_2 (1.00 g), TEA (72.08 μL), and DMF (15 mL) at ambient temperature for 12 h. PS-*g*-OEMPEG as a white solid (1.36 g, 73.5%) was obtained after dialysis against distilled deionized water for 24 h and lyophilization. Meanwhile, PS-*g*-MPEG was synthesized as a white solid in the same way. The amino contents in PS-*g*-OEMPEG and PS-*g*-MPEG were measured by TNBSA assay. Its structure was determined via ^{1}H NMR in DMSO-d_6.

2.6. Formation of blank and DOX-loaded micelles

The polymeric micelles were prepared using a solvent exchange method. To obtain blank micelles, 35 mg of copolymers were dissolved in 2 mL of DMSO and added dropwise into 20 mL of PBS (pH 7.4) under slowly stirring. Afterwards, the mixture was transferred to dialysis bags (MWCO 3500) for dialysis against PBS (pH 8.0) for 24 h. To obtain DOX-loaded micelles (PS-*g*-OEMPEG-DOX and PS-*g*-MPEG-DOX), 45 mg of copolymers and 9 mg of deprotonated DOX were dissolved in 3 mL of DMSO and dialyzed through the same process as that for blank micelles.

2.7. Determination of the critical micelle concentration (CMC)

To measure the concentration at which the copolymers can encapsulate a hydrophobic molecule, the CMC were determined using Nile Red as a probe. The copolymers and Nile Red were mixed in PBS at pH 7.4. The final concentration of Nile Red was 1×10^{-6} mol/L, while the polymeric concentrations varied from 1.0×10^{-7} to 2 mg/mL. A spectrofluorophotometer was used to measure the fluorescence signals at a fixed excitation wavelength of 554 nm with an emission spectrum (550–720 nm). The micellar CMC values were confirmed from plots with polymer concentration and maximum absorption wavelength as

horizontal and vertical coordinate, respectively.

2.8. Determination of micellar DePEGylation

The micellar DePEGylation was determined via the hydrolysis rates of ortho ester linkages in side chains. In brief, the micelles were suspended in PBS (pH 7.4 and 6.5), and lyophilized at desired time points. Afterwards, the lyophilized samples were dissolved in d_6-DMSO and the structural signals were measured via ^{1}H NMR. The peak at 5.84 ppm corresponded to the characteristic proton of ortho esters, and the peaks at 7.98 and 8.24 ppm represented the characteristic protons of hydrolysates of ortho esters. The hydrolysis rates (HR) of ortho esters were calculated as follows: HR (%) = (Integrated areas of peaks at 7.98 and 8.24 ppm)/(Integrated areas of peaks at 5.84, 7.98 and 8.24 ppm).

2.9. Measurement of drug loading content (DLC) and drug loading efficiency (DLE)

To measure the micellar DLC and DLE, the lyophilized drug-loaded micelles with known weight were dissolved in DMSO and optimal absorbance of DOX was recorded at 481 nm by microplate reader (M2e Molecule Devices, USA). DLC and DLE were calculated as follows: DLC (%) = (Weight of the DOX in micelles)/(Weight of the DOX-loaded micelles) × 100%. DLE (%) = (Weight of the DOX in micelles)/(Weight of the feeding drug) × 100%.

2.10. Determination of micellar sizes, zeta potentials and long-term stability

The micellar average diameters were determined via Zetasizer dynamic light scattering detector (DLS) and Transmission Electron Microscope (TEM, JEM-2100, Japan). DLS was also used to evaluate the micellar zeta potentials, long-term stability in SDS solution (20 mg/mL), and particle size changes in the PBS (pH 7.4 and 6.5) with or without DTT (10 mmol/L).

2.11. In vitro pH/reduction-triggered drug release study

Micellar DOX release in the PBS (pH 7.4 and 6.5) with or without DTT (10 mmol/L) were studies via a dialysis method. In brief, micelles-DOX were suspended in 1 mL of PBS and dialyzed against 5 mL of the corresponding PBS at 37 °C. At each time points, all release media were sampled and replaced with another 5 mL of PBS. The amount of DOX released from micelles was calculated via UV–Vis spectroscopy based on a calibration curve prepared in the same buffer.

2.12. In vitro cytotoxicity assay

The MTT assay was used to determine the cytotoxicity of blank and DOX-loaded micelles. In brief, the tumor cells (HepG2 and H22) were seeded in 96-well plates and incubated for 24 h, and then washed and replaced by fresh medium of pH 7.4 and 6.5 respectively. After another 24 h of incubation with various formulations, the cells in each well were added by 20 μL of MTT (5 mg/mL) and incubated for 4 h. Afterwards, the medium was removed and 150 μL of DMSO was added to dissolve the internalized purple formazan crystals. Finally, a microplate reader was used to record the absorbance at 570 nm after the plate was agitated for 15 min.

2.13. Uptake of DOX-loaded micelles

The uptake of various formulations by HepG2 and H22 cells was confirmed on confocal laser scanning microscope (CLSM, FluoView TM FV1000, Olympus) and flow cytometry (BD FACSCalibur), respectively. The cells at 5×10^3 cells/well were plated in 6-well culture plates and cultured for 24 h, following by removing medium and adding various DOX formulations with equivalent DOX concentrations (16 μg/mL) at 37 °C for 4 h. Afterwards, The nuclei labeled with Hoechst 33258 were recorded using CLSM, and the nuclei without dye were recorded by flow cytometry.

2.14. Penetration in HepG2 multicellular spheroids (MCs)

HepG2 MCs were successfully cultured as described previously [25], and the MCs with the diameter about 200–300 μm were picked, and co-cultured with various DOX formulations (8 μg/mL) for predetermined time intervals. Afterwards, the culture medium was removed and MCs were thoroughly washed by PBS before observation. Finally, the treated MCs were imaged and determined by CLSM and Image J. Z-stack, respectively.

2.15. Growth inhibition study in MCs

In brief, about twenty of HepG2 MCs with a diameter approximately 200–250 μm were collected and incubated with each DOX formulation (8 μg/mL) for 5 days respectively, and the diameter of each spheroid was measured and taken image using the optical microscope. All experiments were conducted in triplicate.

2.16. In vivo biodistribution

H22 tumor-bearing ICR mice were randomly divided into four cohorts of 18 mice each. Various DOX formulations (6 mg/kg) and saline were intravenously injected via the tail vein. At each time interval, the mice were sacrificed and the blood samples and major tissues (heart, liver, kidney, lung, spleen and tumor) were collected, weighted, and measured by a microplate reader (Ex = 480 nm, Em = 590 nm) to detect the fluorescence intensity of DOX. The DOX concentration in each sample was calculated based on the standard curves.

2.17. In vivo antitumor effect

For tumor regression study, H22 tumor-bearing mice treated with a single dose were observed for 7 days and given three times for 21 days (one injection every 7 days). The width and length of the tumors and the body weight of mice were measured every day. Tumor volume (V) was calculated as follows: V (mm^3) = 1/2 × length (mm) × width $(mm)^2$. After 7 and 21 days, the mice were sacrificed, and the tumors were collected, weighted and taken image, respectively. Additionally, major tissues (heart, liver, kidney, lung, spleen) and tumors were processed into histological section for mice treated with a single dose after 7 days.

3. Results and discussion

3.1. Preparation and characterization of two PEGylation copolymers and micelleplex systems

To prepare the well-defined PEGylated poly(disulfide)s (PS-*g*-OEMPEG and PS-*g*-MPEG), the disulfide linkages were successfully introduced into the polymeric main-chains via facile polyreaction between 2-hydroxyethyl disulfide, hexamethylene diisocyanate and trifluoroacetylated serinol, and MPEG with or without pH-sensitive ortho ester linkages were grafted in the side chains of poly(disulfide)s respectively via acylation reaction, after trifluoroacetyl were removed from fluorinated poly(disulfide)s (Scheme 2). Polymeric chemical structures were confirmed by ^{1}H NMR spectra (Figs. 1, S1 and S2), and both of PEGylated graft values were determined to be about 20% by TNBSA assay [26]. In addition, two polymeric molecular weights were about 1.45×10^4 g/mol through calculation from the graft degrees, which were similar to that measured by GPC (Table S1).

Two amphipathic PEGylated poly(disulfide)s can readily self-assemble into blank and DOX-loaded micelles via a dialysis method, and

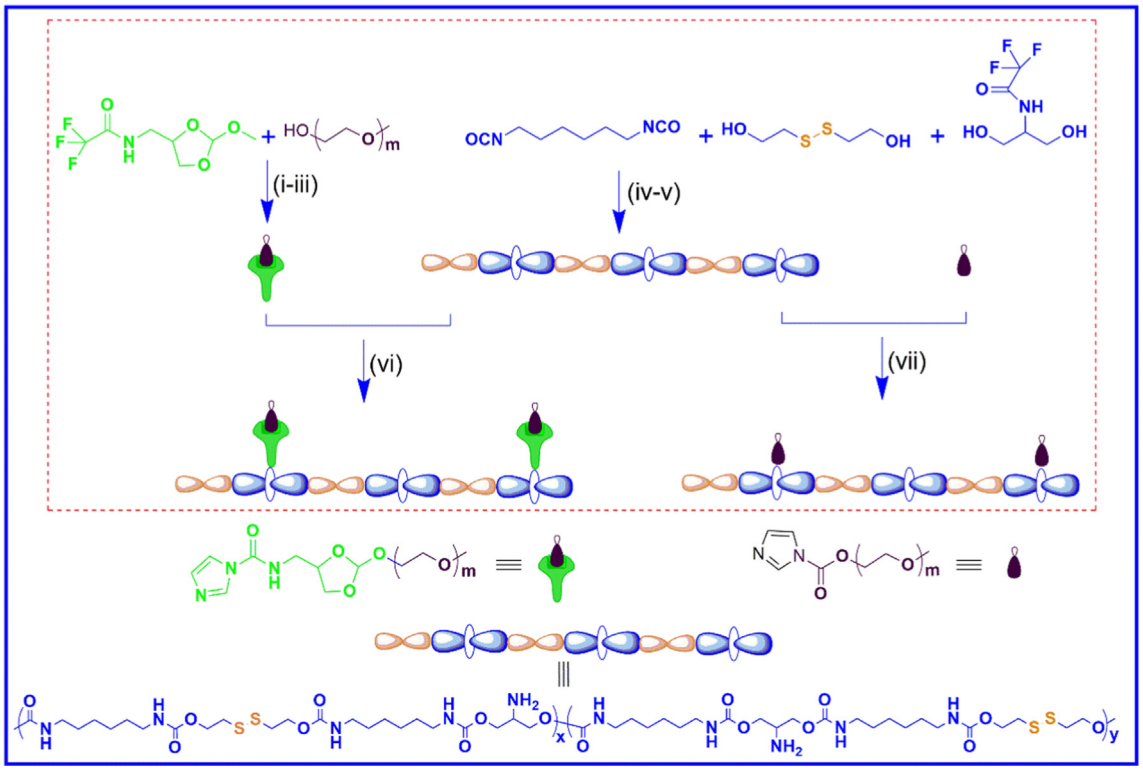

Scheme 2. Synthesis schematic of PEGylated poly(disulfide)s. Reaction condition: (i) Py-PTSA; (ii) 1.00 mol/L NaOH solution; (iii) CDI/TEA; (iv) DBTDL; (v) 7% Na_2CO_3; (vi) TEA; (vii) TEA.

micellar DLC and DLE were confirmed to be about 9% and 80% respectively (Table S2). The micellar CMC values were calculated to be about 10^{-4} mg/mL (Fig. S3), which is considered low and may be beneficial for micellar formation and stable blood circulation. The micellar average hydrodynamic diameters were about 160 nm confirmed by DLS (Fig. 2A and Table S2), which was larger than the average diameters in a drying state observed by TEM (Fig. 2B and C). Moreover, the micellar sizes and count rates could remain unchanged for 48 h in SDS solution (Fig. S4), also indicating their rather stable blood circulation [27]. In addition, micellar zeta potentials (~-15–22 mV)

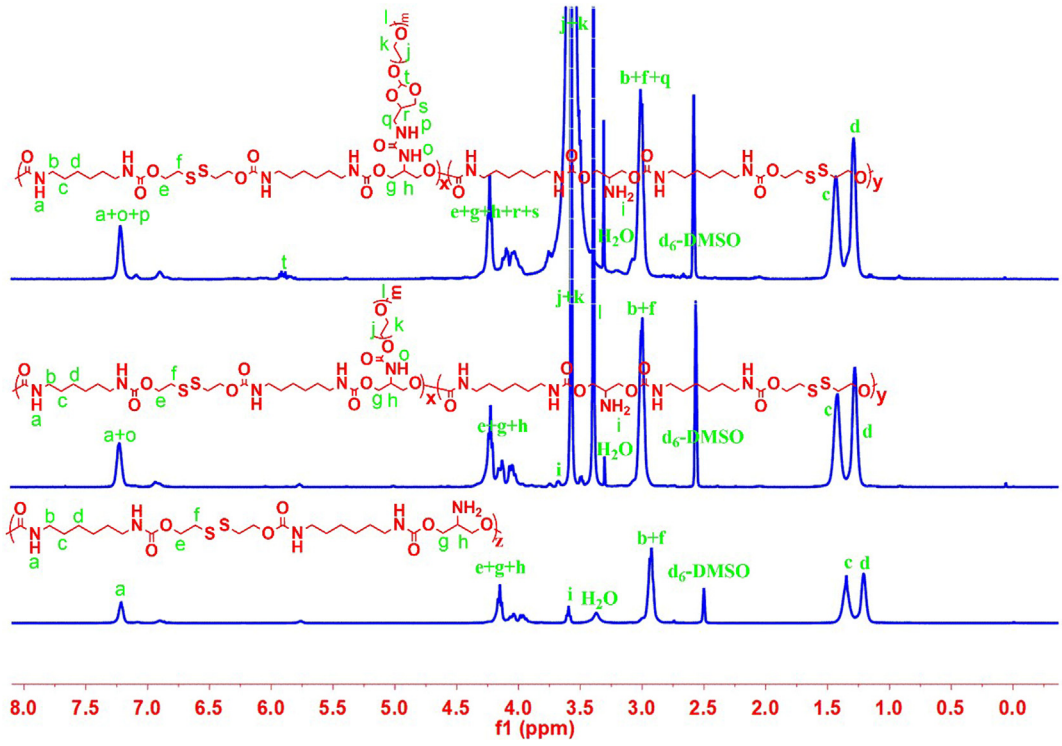

Fig. 1. ^{1}H NMR spectra of PS-*g*-NH_2, PS-*g*-MPEG and PS-*g*-OEMPEG.

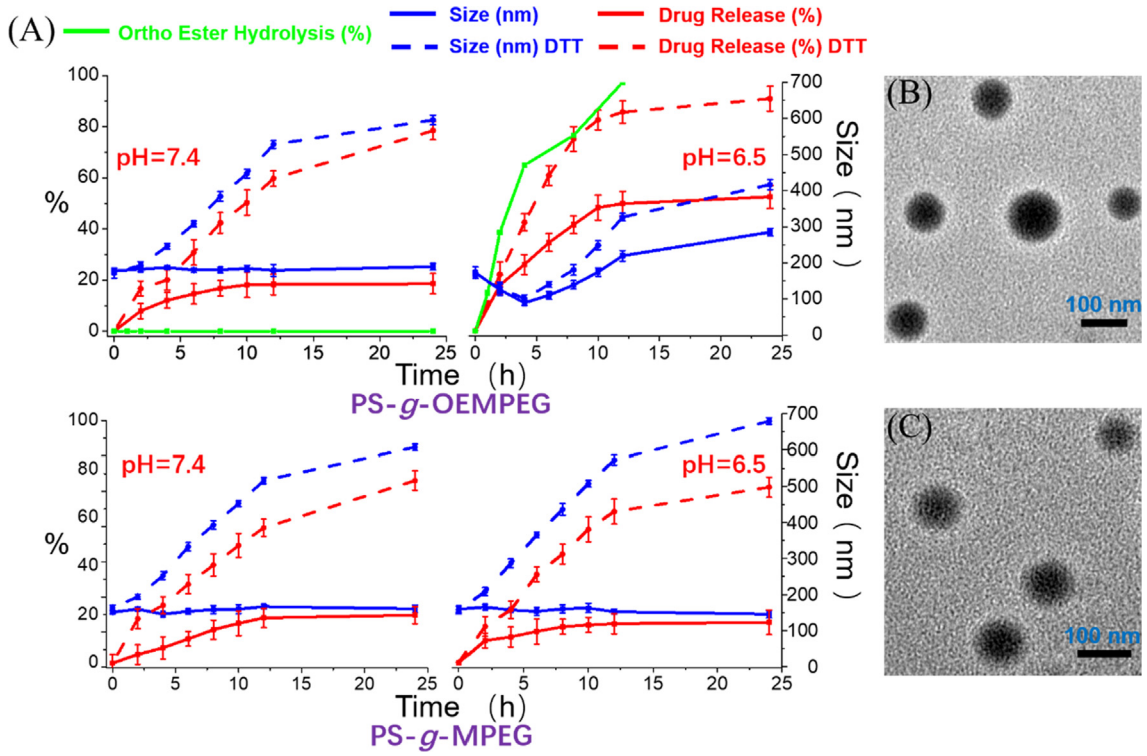

Fig. 2. Kinetics of micellar hydrolysis, size transition and drug release (A) and TEM images of PS-*g*-OEMPEG micelle (B) and PS-*g*-MPEG micelle (C).

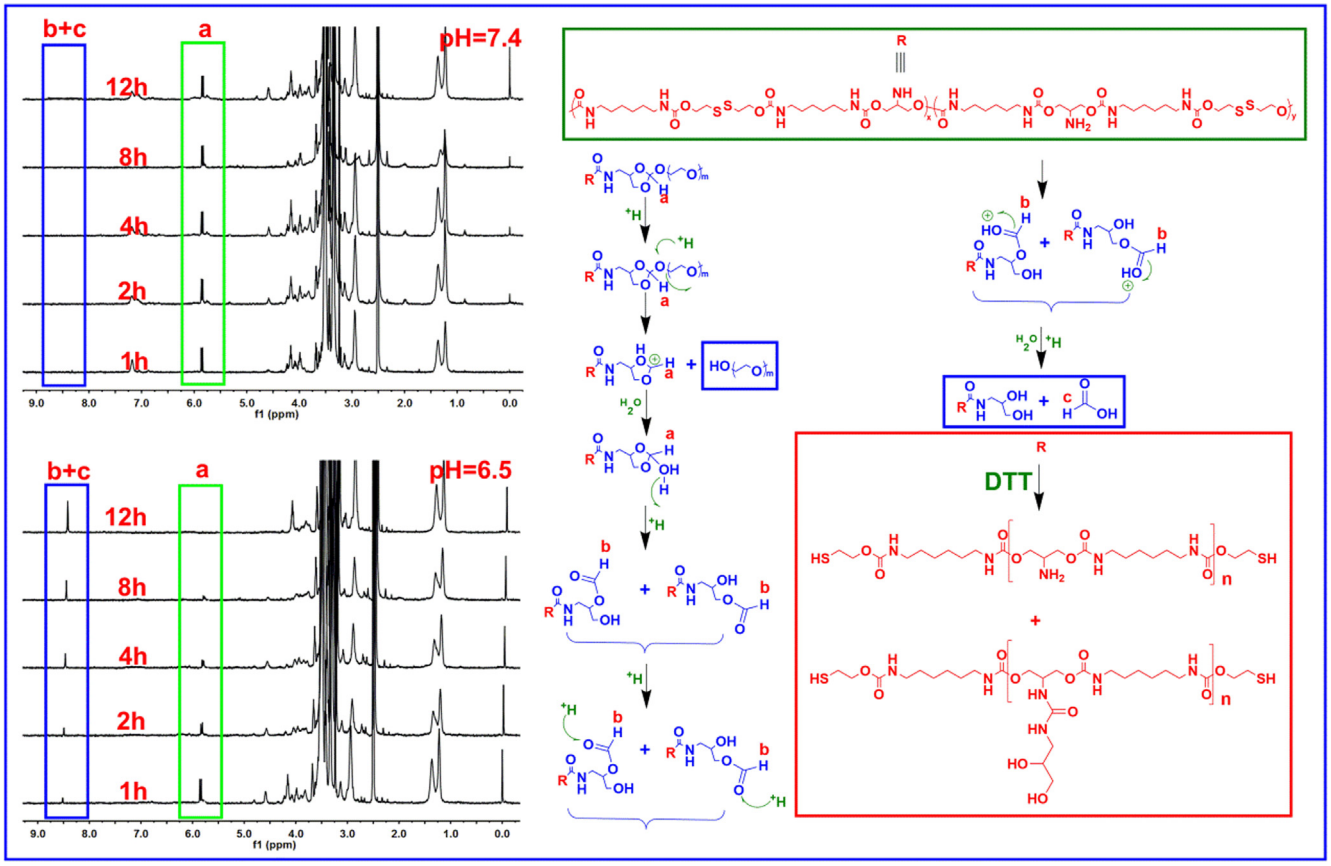

Fig. 3. ^{1}H NMR spectra at pH 7.4 and 6.5 following time course (Peaks labeled with 'a', 'b' and 'c' are protons characteristic of the cyclic ortho ester, formate ester and formate groups, respectively) and hydrolysis mechanism of PS-*g*-OEMPEG micelles.

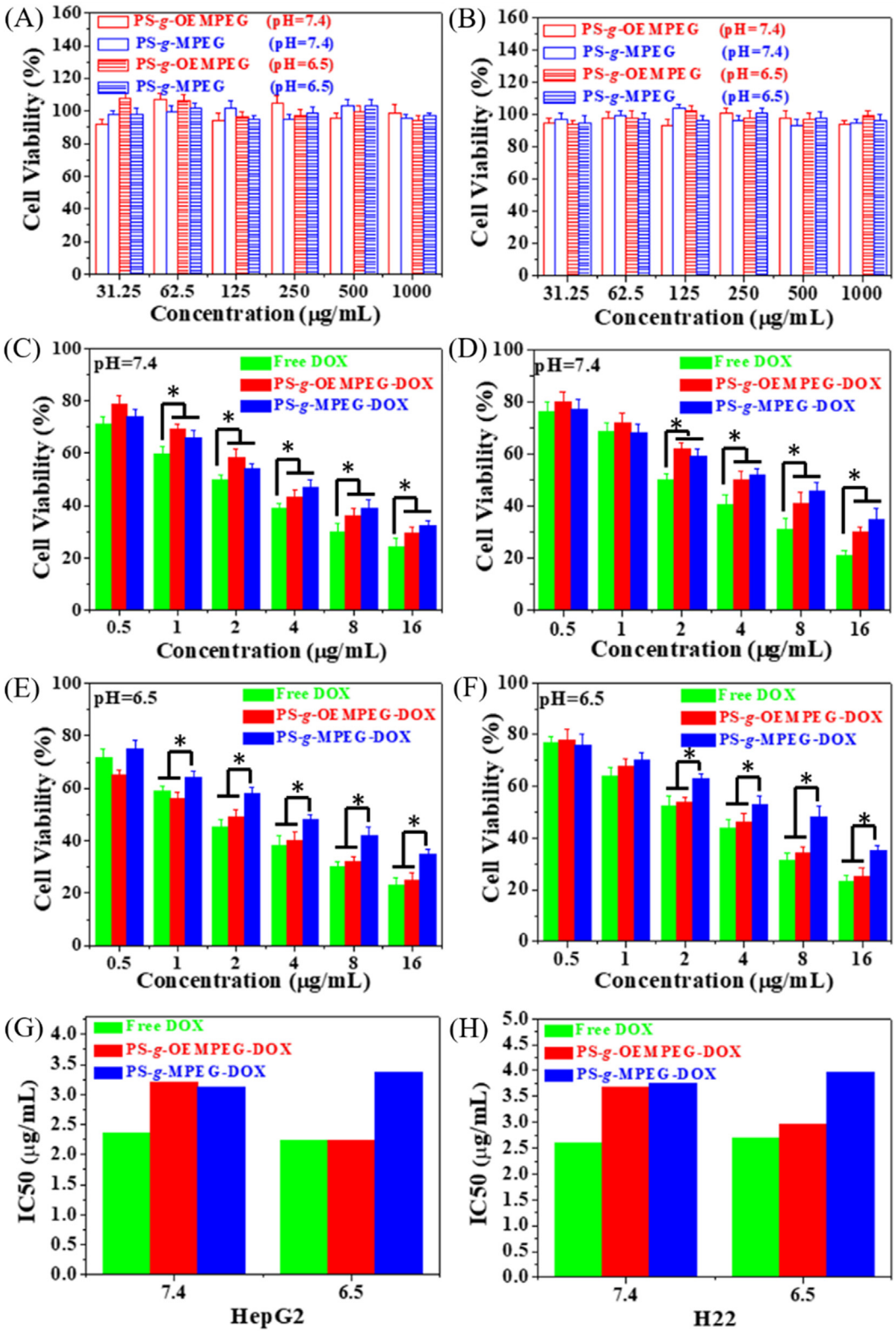

Fig. 4. In vitro cytotoxicity of blank micelles, DOX-loaded micelles and free DOX in HepG2 (A, C and E), and H22 (B, D and F) at different pH values (7.4 and 6.5); IC50 of various DOX formulations in HepG2 (G) and H22 (H) at different pH values (7.4 and 6.5); (*represents $P < 0.05$).

measured by DLS were in the optimal range of stability (Table S3), further suggesting the micellar stable blood circulation [28].

3.2. DePEGyaltion at tumoral extracellular pH value

In order to evaluate the DePEGylation of PS-*g*-OEMPEG in side chains, ^{1}H NMR analysis was performed to determine the hydrolysis of ortho esters in 12 h. As shown in Figs. 2A and 3, the hydrolysis of ortho esters didn't occur in 12 h at pH 7.4, yet was much accelerated at tumoral extracellular pH value (6.5). Moreover, the degradation of ortho esters was quickly accomplished in 12 h. The result proved that the micellar DePEGylation could be realized at tumoral extracellular milieu

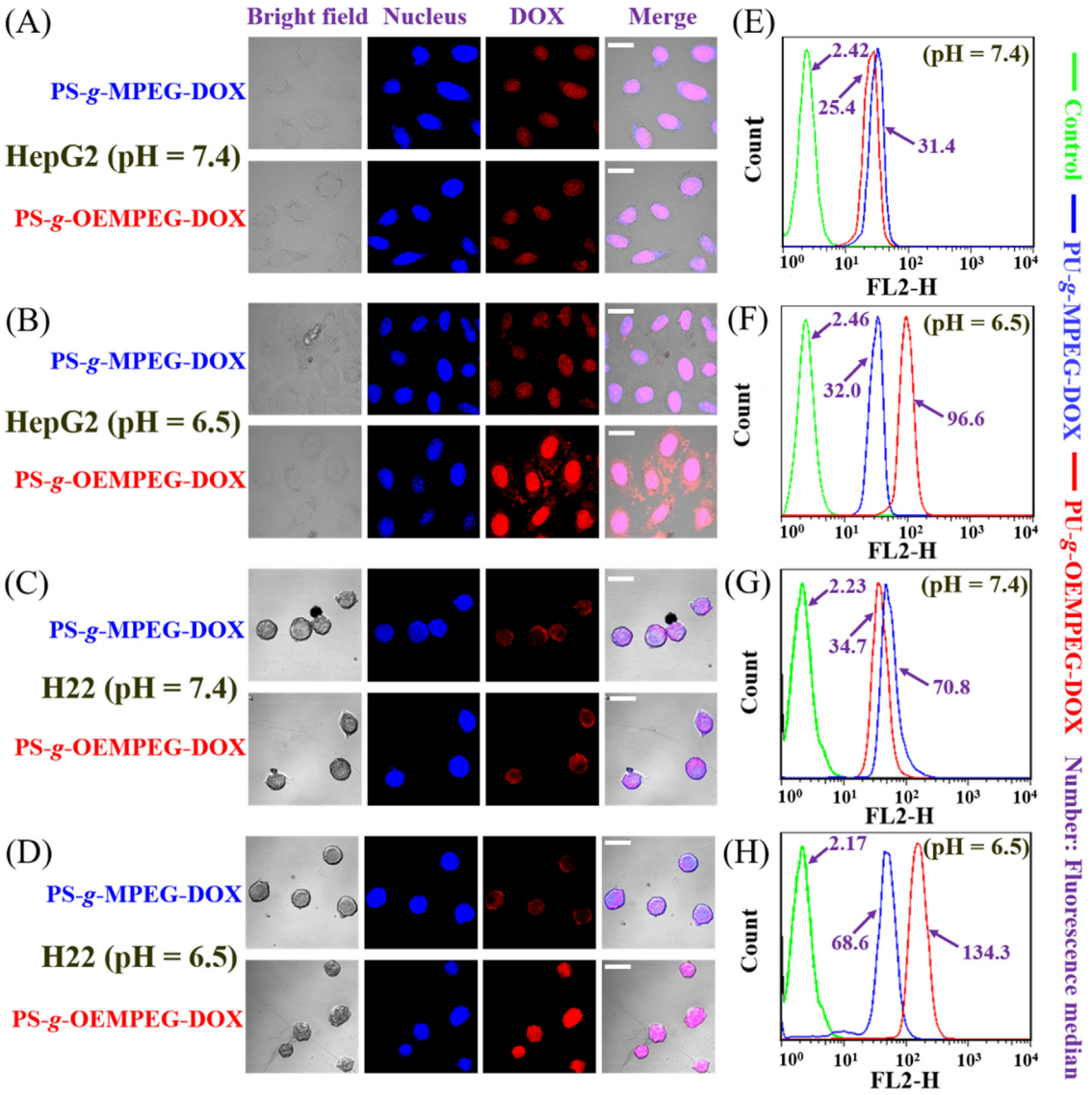

Fig. 5. Cellular uptake of DOX formulations in HepG2 (A, B, E and F) and H22 (C, D, G and H) at different pH values (7.4 and 6.5) confirmed by CLSM and flow cytometry, respectively; Scale bar = 10 μm.

via linking pH-sensitive ortho esters with MPEG in side chains. In addition, as shown in Fig. 3, the hydrolysis of five-membered cyclic ortho esters in side chains yielded formate ester and formate (7.98 ppm and 8.24 ppm), suggesting following a distinct exocyclic mechanism [29–31].

3.3. Dynamic size transition from DePEGylation and degradation of disulfide bonds

The DePEGylation in side chains and cleavage of disulfide bonds in backbone had a great impact on micellar particle sizes (Fig. 2A). The particle sizes of PS-*g*-OEMPEG micelle didn't change in 24 h at pH 7.4, in line with no hydrolysis of ortho esters in side chains at pH 7.4 as revealed by ^{1}H NMR (Figs. 2A and 3). Interestingly, its average sizes had dynamic changes in 24 h at tumoral extracellular pH value (6.5); the sizes gradually decreased to about 75 nm in the first 4 h, possibly due to the increase of hydrophobicity/hydrophily ratio along with the partial DePEGylation, and then gradually increased to about 300 nm in the next 20 h, potentially because of micellar structural instability with further DePEGylation. It's worth noting that the micellar dynamic size changes at pH 6.5 may be conducive to drug accumulation, when initially getting to tumor sites as small nanoparticles for enhanced penetration and then retaining large nanoparticles within tumors for improved retention [14,15,32]. In addition, owing to the degradation of disulfide bonds in micellar cores in the presence of DTT (Fig. 3), two micellar sizes became gradually larger whether at pH 7.4 or 6.5, which was likely to trigger intracellular rapid drug release.

3.4. Drug release depending on intracellular reduction environment

Micellar DOX release exhibited obviously reduction dependence (Fig. 2A). In the absence of DTT, only approximately 20% of DOX was released from two micelles at pH 7.4 and PS-*g*-MPEG-DOX at pH 6.5 in 24 h. In the presence of DTT, however, the amount of drug release was much accelerated and reached 80–95% for micelles-DOX at different pH values. Such higher amount of drug release mainly resulted from the micellar gradual swelling with loose structure, along with degradation of disulfide bonds in the micellar cores. Moreover, the efficiently intracellular drug release can benefit rapid cell-killing ability. In addition, the drug release of PS-*g*-OEMPEG-DOX was at a low level at pH 6.5, and might be lower in vivo on account of the gradually decreased pH (7.0–6.5) distribution within tumors [5].

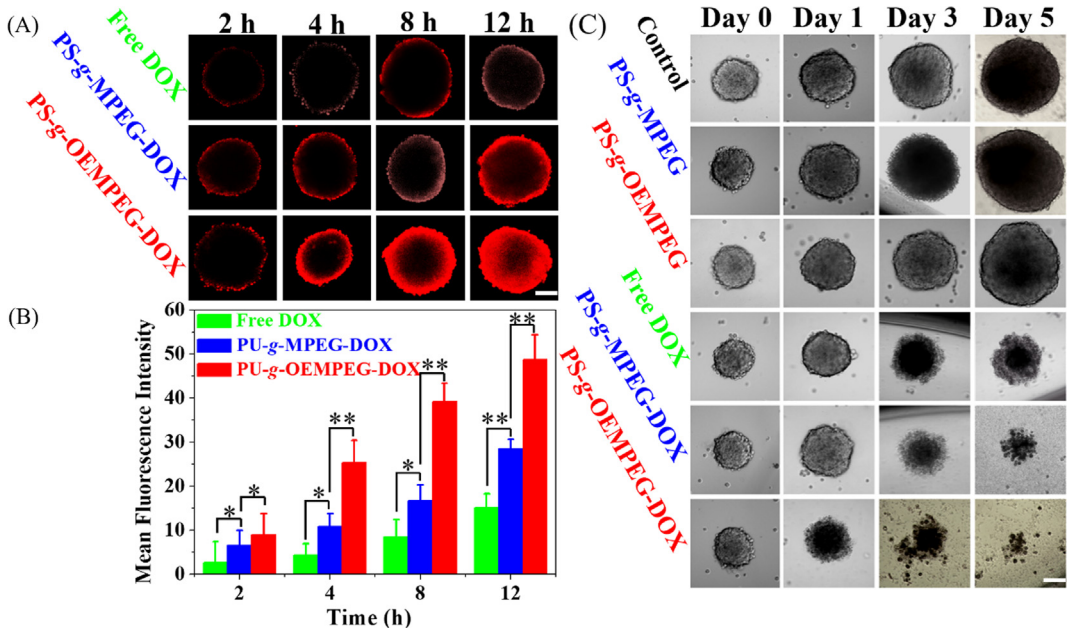

Fig. 6. (A) Penetration in HepG2 MCs photographed by CLSM. (B) Mean fluorescence intensities of various DOX formulations in HepG2 MCs. (C) Growth inhibition of HepG2 MCs by formulations. Scale bars = 100 μm; (*represents $P < 0.05$ and **represents $P < 0.01$).

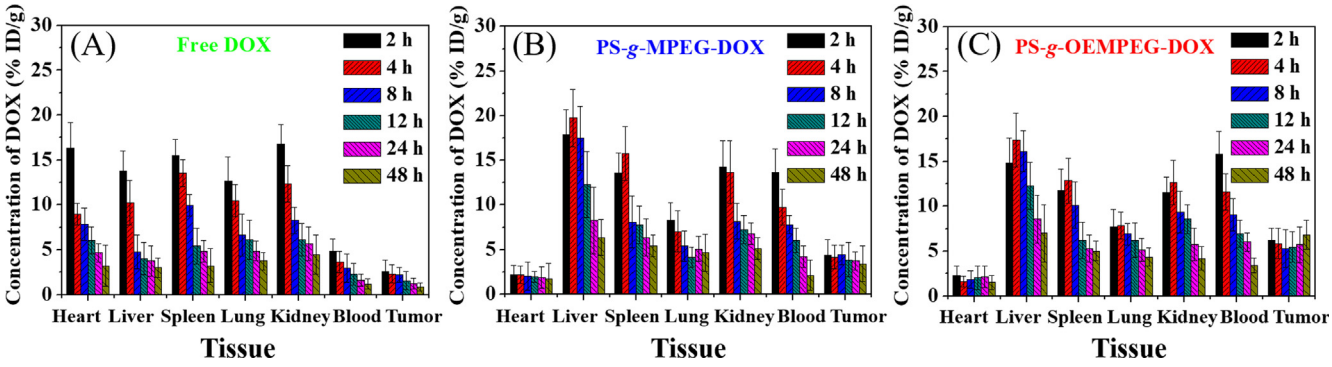

Fig. 7. In vivo biodistribution of various DOX formulations in H22 tumor-bearing mice.

3.5. Enhanced cytotoxicity and cellular uptake via DePEGylation

MTT assay was performed to investigate the effect of micellar detachable PEGylation on pharmacological activity, using two types of cancer cells (HepG2 and H22) at pH 7.4 and 6.5 for 24 h, respectively. Meanwhile, blank micelles also co-cultured with HepG2 and H22. As displayed in Fig. 4A and B, the blank micelles exhibited no cytotoxicity to two type cells. As seen in Fig. 4C–H, the DOX formulations showed distinct dose-dependent cytotoxicity, and the cytotoxicity of PS-*g*-OEMPEG-DOX was similar with that of PS-*g*-MPEG-DOX, but significantly lower than that of free DOX at pH 7.4. On the other hand, the cytotoxicity of PS-g-OEMPEG-DOX was significantly higher than that of PS-g-MPEG-DOX, and similar with that of free DOX at pH 6.5. The result demonstrated that the micellar DePEGylation could significantly improve cell-killing ability. In addition, we further evaluated the effect of micellar detachable PEGylation on cellular uptake by comparison with their cellular internalization at pH 7.4 and 6.5 via confocal fluorescence microscopy and flow cytometry, respectively. As displayed in Fig. 5A–H, the intracellular fluorescence intensity or median of PS-*g*-OEMPEG-DOX was slightly lower than that of PS-*g*-MPEG-DOX at pH 7.4 due to its larger particle sizes, but higher at pH 6.5 owing to its DePEGyation [10–13]. Thus, these results suggested that the improved cytotoxicity of PS-*g*-OEMPEG-DOX at tumoral extracellular pH was attributed to its enhanced cellular internalization via extracellular DePEGylation [10–13]. In addition, free DOX had strong cytotoxicity in the experiment, because small molecule cationic drugs could easily be internalized by cells [5].

3.6. Penetration in HepG2 multicellular spheroids (MCs)

MCs have been reported a lot to estimate tumor uptake and penetration in vitro [25], and CLSM was used here to determine the fluorescence of DOX in HepG2 MCs. As displayed in Fig. 6A and B, the fluorescence signals of free DOX and PS-*g*-MPEG-DOX distributed just within the periphery of MCs in the first 4 h, and distributed only about 50 and 150 μm respectively from the outer layers to the center of MCs after 12 h. Interestingly, PS-*g*-OEMPEG-DOX could quickly penetrate into the center of MCs in the first 4 h, although the fluorescence signals in the center were weak. Moreover, it could be observed that strong fluorescence signals distributed from the periphery toward the center after 8 h, and almost occupied the entire MCs after 12 h. The results suggested that PS-*g*-OEMPEG-DOX had stronger tumor penetration than other DOX formulations. This was possibly because free DOX as small molecule cationic drugs was easily adsorbed with the negatively charged extracellular matrix in the outer layers of MCs and could not readily diffuse into the cores of the MCs [5]; yet PS-*g*-OEMPEG-DOX, with dynamic size changes (large-to-small-to-large size transitions) via gradual DePEGylation at tumoral extracellular milieu, could much

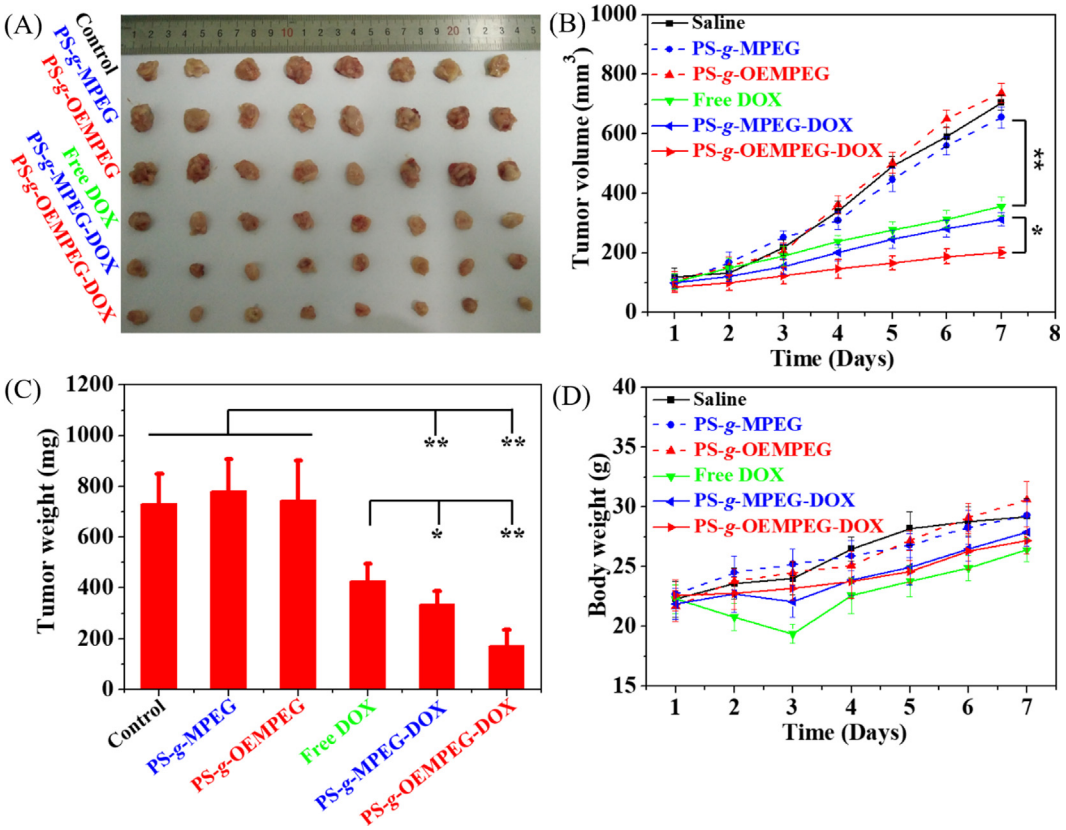

Fig. 8. Tumor image (A) and weight (C) of mice after treatment for 7 days. Change trends in tumor volume (B) and body weight (D) of mice following 7 days. (*represents $P < 0.05$ and **represents $P < 0.01$).

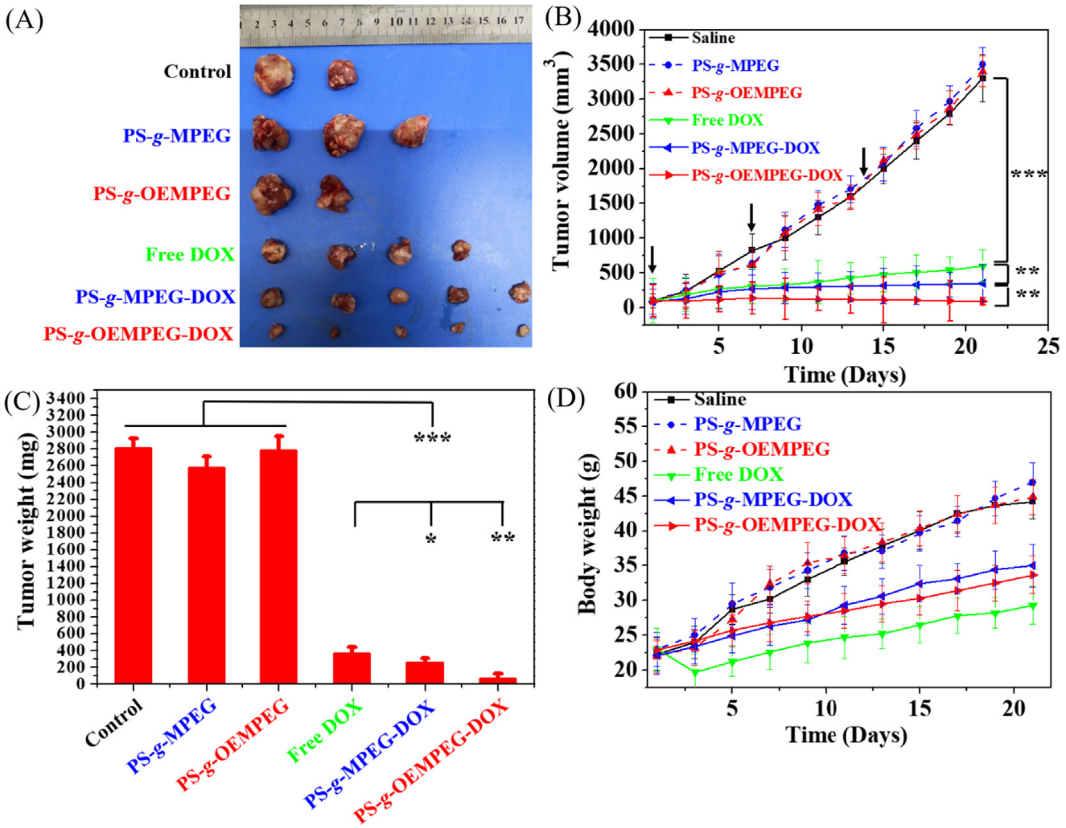

Fig. 9. Tumor image (A) and weight (C) of mice after treatment for 21 days. Change trends in tumor volume (B) and body weight (D) of mice following 21 days. (*represents $P < 0.05$, **represents $P < 0.01$ and ***represents $P < 0.001$).

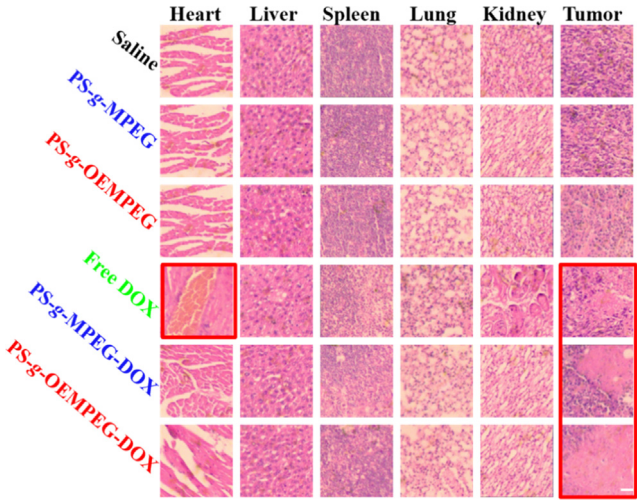

Fig. 10. Images of the histological sections through a single administration; Scale bar = 500 μm.

more easily infiltrate into the tumor matrix in comparison with free DOX and PS-*g*-MPEG-DOX [14,15,32].

3.7. Growth inhibition of HepG2 MCs

Various DOX formulations, the culture medium and blank micelles were exposed to HepG2 MCs for 5 days to compare their tumor inhibition in vitro. As seen in Fig. 6C, the culture medium and blank micelles without cytotoxicity failed to limit tumor growth and the MCs gradually largened day by day. However, all DOX formulations could efficiently inhibit the growth of MCs and make their volumes smaller day by day. Among them, the free DOX and PS-*g*-MPEG-DOX limited tumor growth mainly through killing tumor cells in the outer layers, but PS-*g*-MPEG-DOX destructed MCs through cytotoxicity from the periphery toward the center. That is why the outer layers of MCs become loose for free DOX and PS-*g*-MPEG-DOX groups and the enter MCs become loose for PS-*g*-OEMPEG-DOX group after 3 days. Furthermore, PS-*g*-OEMPEG-DOX turned out to be the best tumor inhibition in all DOX formulations after 5 days. The results agreed well with its stronger tumor penetration of MCs in vitro, suggesting that tumoral extracellular DePEGylation and dynamic size transitions and intracellular rapid drug release could be beneficial for tumor inhibition.

3.8. In vivo biodistribution

To evaluate the effect of micellar detachable PEGylation on in vivo drug biodistribution, various DOX formulations were injected into the H22 tumor-bearing mice via i.v. administration. As displayed in Fig. 7, the results clearly indicated that the DOX concentrations in each tissue varied with different DOX formulations. The amount of DOX in micelles was obviously lower in heart and lung tissues, but higher in blood than that of free DOX. Moreover, PS-*g*-OEMPEG-DOX obtained the highest tumoral drug concentration in all DOX formulations, possibly owing to its stable circulation, enhanced drug penetration and retention via detachable PEGylation and dynamic size change at tumor tissues [10,14,15].

3.9. Tumor growth inhibition in vivo

To verify the in vivo antitumor ability of the micelle with detachable PEGylation, ICR mice bearing tumors treated with a single dose were observed for 7 days and given three times for 21 days (one injection every 7 days), respectively. Treatment began when the tumor volumes were up to about 100 mm^3 in all mice. Saline, blank micelles, and DOX formulations (6 mg/kg) were administered via tail vein, respectively, and the injection date was labeled as day 1. The tumor volumes and the body weights of the mice were measured every day, and the tumors were surgically removed, weighed and taken images at the end of the treatment. As seen in Figs. 8A–C and 9A–C, all DOX formulations obviously restrained tumor growth compared to the control and blank micelles, and PS-*g*-OEMPEG-DOX achieved the best tumor inhibition whether through a single administration or three times, and stronger destruction of tumor tissue through a single administration (Fig. 10). It was probably owing to its efficient tumor accumulation and cytotoxicity to tumor cells. In addition, mice injected with free DOX exhibited a considerable weight loss compared to other groups, suggesting high toxicity of the free drug at these doses (Figs. 8D, 9D and 10). It is possibly attributed to the nonspecific interactions and recognition of free DOX with normal organs, especially heart [28]. More importantly, as seen in Fig. S5, H22 tumor-bearing mice treated with DOX-loaded micelles exhibited notably greater lifespan enhancement by comparison with other groups.

4. Conclusions

Two well-defined amphipathic PEGylated poly(disulfide)s (PS-*g*-MPEG and PS-*g*-OEMPEG) were successfully constructed via facile polycondensation and grafting reaction in turn, and could self-assemble into blank and DOX-loaded micelles. PS-*g*-OEMPEG micelle exhibited stable circulation in SDS solution at pH 7.4, DePEGylation and dynamic size transitions via hydrolysis of ortho ester linkages in side chains at tumoral extracellular pH value (6.5), and effective drug release via cleavage of disulfide bonds in the backbone. PS-*g*-OEMPEG-DOX had stronger cellular internalization and cytotoxicity at tumoral extracellular pH value (6.5), and stronger penetration and inhibition of MCs in vitro. Moreover, in vivo biodistribution and tumor inhibition examination showed that PS-*g*-OEMPEG-DOX had higher blood and tumoral drug concentrations and could restrain tumor growth while decreasing side effects in normal organs. Therefore, the sequentially dynamic polymeric micelle with detachable PEGylation and intracellular rapid drug release can serve as a promising prototype in clinic cancer treatment.

Declaration of Competing Interest

The authors declared that there is no conflict of interest.

Acknowledgments

This work is financially supported by the National Natural Science Foundation of China (No. 51803001, 51603001 and 51503001), the Research Foundation of Education Department of Anhui Province of China (No. KJ2018ZD003 and KJ2018A0006), and the Academic and Technology Introduction Project of Anhui University (AU02303203).

Appendix A. Supplementary material

Supplementary data to this article can be found online at https://doi.org/10.1016/j.ejpb.2019.10.009.

References

[1] T. Ramasamy, H.B. Ruttala, B. Gupta, B.K. Poudel, H. Choi, C.Y. Yong, J.O. Kim, Smart chemistry-based nanosized drug delivery systems for systemic applications: a comprehensive review, J. Control. Release 258 (2017) 226–253.
[2] H. Li, H. Jin, W. Wan, C. Wu, L. Wei, Cancer nanomedicine: mechanisms, obstacles and strategies, Nanomedicine 13 (2018) 1639–1656.
[3] A. Wicki, D. Witzigmann, V. Balasubramanian, J. Huwyler, Nanomedicine in cancer therapy: challenges, opportunities, and clinical applications, J. Control. Release 200 (2015) 138–157.
[4] Y.S. Youn, Y.H. Bae, Perspectives on the past, present, and future of cancer nanomedicine, Adv. Drug Deliv. Rev. 130 (2018) 3–11.

[5] V.P. Chauhan, R.K. Jain, Strategies for advancing cancer nanomedine, Nat. Mater. 12 (2013) 958–962.
[6] Q. Sun, Z. Zhou, N. Qiu, Y. Shen, Rational design of cancer nanomedicine: nanoproperty integration and synchronization, Adv. Mater. 29 (2017) 1606628.
[7] A. Gabizon, H. Shmeeda, Y. Barenholz, Pharmacokinetics of pegylated liposomal doxorubicin, Clin. Pharmacokinet. 42 (2003) 419–436.
[8] H. Otsuka, Y. Nagasaki, K. Kataoka, PEGylated nanoparticles for biological and pharmaceutical applications, Adv. Drug Deliv. Rev. 64 (2012) 246–255.
[9] K. Knop, R. Hoogenboom, D. Fischer, U.S. Schuber, Poly(ethylene glycol) in drug delivery: pros and cons as well as potential alternatives, Angew. Chem. Int. Ed. 49 (2010) 6288–6308.
[10] L. Kong, F. Campbell, A. Kros, DePEGylation strategies to increase cancer nanomedicine efficacy, Nanosc. Horiz. 4 (2019) 378–387.
[11] C.Y. Sun, S. Shen, C.F. Xu, H.J. Li, Y. Liu, Z.T. Cao, X.Z. Yang, J.X. Xia, J. Wang, Tumor acidity-sensitive polymeric vector for active targeted siRNA delivery, J. Am. Chem. Soc. 137 (2015) 15217–15224.
[12] X. Guan, Z. Guo, T. Wang, L. Lin, J. Chen, H. Tian, A pH-responsive detachable PEG shielding strategy for gene delivery system in cancer therapy, Biomacromolecules 18 (2017) 1342–1349.
[13] C. Sun, Y. Liu, J. Du, Z. Cao, C. Xu, J. Wang, Facile generation of tumor-pH-labile linkage-bridged block copolymers for chemotherapeutic delivery, Angew. Chem. Int. Ed. 55 (2016) 1010–1014.
[14] Q. Sun, X. Sun, X. Ma, Z. Zhou, E. Jin, B. Zhang, Y. Shen, E.V. Kirk, W. Murdoch, J. Lott, T. Lodge, M. Radosz, Y. Zhao, Integration of nanoassembly functions for an effective delivery cascade for cancer drugs, Adv. Mater. 26 (2014) 7615–7621.
[15] H.J. Li, J.Z. Du, X.J. Du, C.F. Xu, C.Y. Sun, H.X. Wang, Z.T. Cao, X.Z. Yang, Y.H. Zhu, S.M. Nie, J. Wang, Stimuli-responsive clustered nanoparticles for improved tumor penetration and therapeutic efficacy, Proc. Natl. Acad. Sci. USA 113 (2016) 4164–4169.
[16] G. Yan, J. Wang, L. Hu, X. Wang, G. Yang, S. Fu, X. Cheng, P. Zhang, R. Tang, Stepwise targeted drug delivery to liver cancer cells for enhanced therapeutic efficacy by galactose-grafted, ultra-pH-sensitive micelles, Acta Biomater. 51 (2017) 363–373.
[17] G. Yan, J. Wang, P. Zhang, L. Hu, X. Wang, G. Yang, S. Fu, X. Cheng, R. Tang, Tunable dynamic fluorinated poly(orthoester)-based drug carriers for greatly enhanced chemotherapeutic efficacy, Polym. Chem. 8 (2017) 2063–2073.
[18] G. Yan, Q. Zha, J. Wang, X. Wang, X. Cheng, W. Yao, R. Tang, Dynamic, ultra-pH-sensitive graft copolymer micelles mediated rapid, complete destruction of 3-D tumor spheroids in vitro, Polymer 111 (2017) 192–203.
[19] G. Yan, J. Wang, J. Qin, L. Hu, P. Zhang, X. Wang, R. Tang, Well-defined poly(ortho ester amides) for potential drug carriers: probing the effect of extra- and intracellular drug release on chemotherapeutic efficacy, Macromol. Biosci. 17 (2017) 1600503.
[20] B. Deng, P. Ma, Y. Xie, Reduction-sensitive polymeric nanocarriers in cancer therapy: a comprehensive review, Nanoscale 7 (2015) 12773–12795.
[21] H. Sun, Y. Zhang, Z. Zhong, Reduction-sensitive polymeric nanomedicines: An emerging multifunctional platform for targeted cancer therapy, Adv. Drug Deliv. Rev. 132 (2018) 16–32.
[22] X. Guo, Y. Cheng, X. Zhao, Y. Luo, J. Chen, W. Yuan, Advances in redox-responsive drug delivery systems of tumor microenvironment, J. Nanobiotechnol. 16 (2018) 74.
[23] G. Wu, Y. Fang, S. Yang, J.R. Lupton, N.D. Turner, Glutathione metabolism and its implications for health, J. Nutr. 134 (2004) 489–492.
[24] M. Yu, L. Zhang, J. Wang, R. Tang, G. Yan, Z. Cao, X. Wang, Acid-labile poly(ortho ester amino alcohols) by ring-opening polymerization for controlled DNA release and improved serum tolerance, Polymer 96 (2016) 146–155.
[25] X. Wang, C. Yang, Y. Zhang, X. Zhen, W. Wu, X. Jiang, Delivery of platinum (IV) drug to subcutaneous tumor and lung metastasis using bradykinin-potentiating peptide-decorated chitosan nanoparticles, Biomaterials 35 (2014) 6439–6453.
[26] Q. Cheng, Y. Huang, H. Zheng, T. Wei, S. Zheng, S. Huo, X. Wang, Q. Du, X. Zhang, H.Y. Zhang, X.J. Liang, C. Wang, R. Tang, Z. Liang, The effect of guanidinylation of PEGylated poly(2-aminoethyl methacrylate) on the systemic delivery of siRNA, Biomaterials 34 (2013) 3120–3131.
[27] N. Kang, M.E. Perron, R.E. Prud'homme, Y. Zhang, G. Gaucher, J.C. Leroux, Stereocomplex block copolymer micelles: core-shell nanostructures with enhanced stability, Nano Lett. 5 (2005) 315–319.
[28] Y. Yang, S.X. Yuan, L.H. Zhao, C. Wang, J.S. Ni, Z.G. Wang, C. Lin, M.C. Wu, W.P. Zhou, Ligand-directed stearic acid grafted chitosan micelles to increase therapeutic efficacy in hepatic cancer, Mol. Pharm. 12 (2015) 644–652.
[29] X. Huang, F. Du, D. Liang, S. Lin, Z. Li, Stereochemical effect of trans/cis isomers on the aqueous solution properties of acid-labile thermoresponsive polymers, Macromolecules 41 (2008) 5433–5440.
[30] J. Heller, J. Barr, Poly (ortho esters) from concept to reality, Biomacromolecules 5 (2004) 1625–1632.
[31] J. Heller, J. Barr, S.Y. Ng, K.S. Abdellauoi, R. Gurny, Poly(ortho esters): synthesis, characterization, properties and uses, Adv. Drug. Deliv. Rev. 54 (2002) 1015–1039.
[32] R. Tang, W. Ji, C. Wang, Amphiphilic block copolymers bearing ortho ester sidechains: pH-dependent hydrolysis and self-assembly in water, Macromol. Biosci. 10 (2010) 192–201.